International Journal of Mechanical, Industrial and Aerospace Sciences
ISSN: 2517-9950
Vol:9, No:10, 2015

Fracture Control of the Soda-Lime Glass in Laser Thermal Cleavage

Jehnming Lin

***Abstract*—**The effects of the contact ball-lens on the soda lime glass in laser thermal cleavage with a cw Nd-YAG laser were investigated in this study. A contact ball-lens was adopted to generate a bending force on the crack formation of the soda-lime glass in the laser cutting process. The Nd-YAG laser beam (wavelength of 1064 nm) was focused through the ball-lens and transmitted to the soda-lime glass, which was coated with a carbon film on the surface with a bending force from a ball-lens to generate a tensile stress state on the surface cracking. The fracture was controlled by the contact ball-lens and a straight cutting was tested to demonstrate the feasibility. Experimental observations on the crack propagation from the leading edge, main section and trailing edge of the glass sheet were compared with various mechanical and thermal loadings. Further analyses on the stress under various laser powers and contact ball loadings were made to characterize the innovative technology.

The results show that the distributions of the side crack at the leading and trailing edges are mainly dependent on the boundary condition, contact force, cutting speed and laser power. With the increase of the mechanical and thermal loadings, the region of the side cracks might be dramatically reduced with proper selection of the geometrical constrains. Therefore the application of the contact ball-lens is a possible way to control the fracture in laser cleavage with improved cutting qualities.

***Keywords*—**Laser cleavage, controlled fracture, contact ball lens.

I. Introduction

LASER can be focused as a cutting tool to achieve a high energy density without the tool contact on the specimen. Since the laser machining has the flexibility for the rapid change of the product design and manufacturing, it is suitable for the process automation in the modern industry. In comparison with the conventional technologies, laser machining is one of the popular applications of the laser materials processing. According to the extraordinary cutting performance of the brittle materials by the laser beam in laser cleaving process, many studies have been carried out in literature. Normally the conventional cutting tool applied for the glass sheet was diamond tip, but the tool contact will cause a rapid wear and combine with rough cutting edges of the glass. Due to the heating with laser irradiation on the glass surface, the thermal stress state could be generated of the surface cracking on glass. Based on the moving path of the laser heating, the thermal cracking can be controlled in various ways, and the laser cleavage method can replace many conventional machining processes such as diamond cutting for the glass. Alternatively, the laser cutting might generate a thermal stress on the glass sheet and cleave the glass surface with a following crack penetration under a mechanical loading, and it has successfully applied to cut the brittle materials such as ceramics and silicon wafers.

Many attempts have been made for the fracture control on brittle materials such as ceramics and glasses by laser cutting [1]-[5], Tsai et al. have studied the crack propagation of the ceramic substrate when cutting curves and asymmetrical straight lines. They found that the extension of the breaking frontier is larger than the movement of the laser spot, the actual fracture trajectory deviates from the desired trajectory [1]. Miyashita et al. [2] used a Nd-YAG laser to cut the soda lime glass with a continuous laser power of 500W and cutting speed of 20mm/s. The crack tip propagated after the turning point about 1.4 mm and formed a circular arc in another direction. They also use the finite element method to prove that the maximum tangential stress intensity factor $K\theta max$ is an important parameter to control the crack growth. Tsai et al. [3] used a bending device on the glass sheet to break the glass sheet after the laser passing. A three-point bending device was clamped on the glass sheet so that the surface can be machined in a tensile stress state, then the crack propagation velocity was increased with a controlled deflection. More recently the control of the fracture of the straight line cutting with pulsed diode laser has been made by [4], [5]. They have investigated the crack formation on the soda-lime glass cleaved by diode lasers [4]. The control of the deviation of the crack from the cutting path at the leading and tailing edges has been made by pulsed laser radiation to minimize the cut path deviation by reducing thermal stresses at optimum laser parameters, and the stress state has been simulated by FEM to verify this effect. Furthermore, they found the thermal stresses generated during laser scanning are strongly dependent upon laser beam geometry [5], and their work also shows that the beam divergence inside the glass plays a significant role in the cutting path deviation at the edges of the glass.

The laser beam was applied to the glass cutting as a heat source. The heat was diffused into the glass from laser spot and dissipated into the surroundings. Thus, the stress state was generated on the substrate surface to initiate the cracks, and the crack progressively followed with the laser beam [6].

The laser path might not consistent with the crack propagation in the laser cleavage of the brittle materials; therefore, an innovative method was proposed to overcome the problem in the present study. A laser beam transmits through a contact ball-lens in a straight-line cutting to improve the crack control in the laser cleavage process. The ball-lens with a contact force was used to bend the glass sheet in laser cleavage.

Jehnming Lin is with the Department of Mechanical Engineering, National Cheng Kung University, Tainan, Taiwan 70101 (phone: 886-6-276-2636; fax: 886-6-235-2973; e-mail:linjem@mail.ncku.edu.tw).

Due to the bending moment, a stress state might enhance the crack tip generated by thermal stress on the surface heated by laser beam and the crack continuously propagates in the laser beam direction. Stress analyses were made to characterize the process for the further applications.

II. Experiment

The experimental arrangement is illustrated in Fig. 1. A cw TEM00 Nd-YAG laser with a wavelength of 1064 nm was focused through a convex silica lens and a BK7 ball-lens to irradiate on a soda-lime glass at a beam spot diameter of ao on the bottom surface, where was coated with a carbon film of the thickness about 6 μm to increase the laser absorption up to 79%. The properties of the silica and BK7 les are listed in Table I [7]. The soda-lime glass substrate with the dimensions of 76 mm x 25mm x 1 mm was used in the experiment. Since the laser beam with a wavelength of 1064 nm through the soda-lime glass is considered as a high transmittance and approximate 8% will be absorbed [8], therefore the heat affected zone is mainly on the bottom surface coated with the carbon film. As illustrated in Fig. 1 (b), two lateral edges of the glass specimen were clamped at a fixture with a grove of 10 mm in width and the ball-lens was pre-loaded by a contact force on the upper surface of the glass to create a bending moment on the glass substrate, where the ball-lens was contacted to the upper surface of the glass specimen. According to the loading force Fe from the ball-lens on the glass substrate, it will generate a bending moment M+ towards the ball-lens and distribute a tensile stress state on the bottom surface of the substrate [9]. Therefore, the tensile stress combined with the thermal stress on the heating zone due to the laser absorption by the carbon film on the bottom surface, the glass sheet will be cleaved with both mechanical and thermal loading in the crack propagation control.

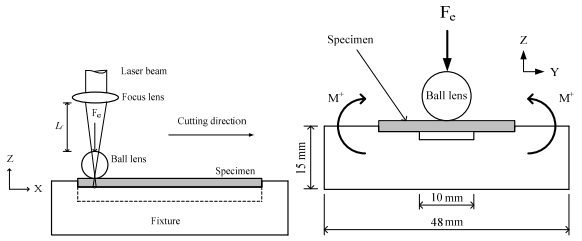

(a) (b)

Fig. 1 (a) Nd-YAG laser thermal cleavage with a contact ball-lens (b) Transverse cross-section view of the cutting front, where the laser cutting direction is along the x axis

The ball-lens system is illustrated in Fig. 2 and there are two sets of the ball-lens (lens radius RL of 5 and 8 mm) adopted in the present study. The analysis of the beam spot diameter was made by ZEMAX software. According to the stand-off distance Ls between the focusing lens and ball-lens as illustrated in Fig. 2 (b), the diameter of the beam spot ao on the substrate surface coated with a carbon film was calculated. Without considering the reflection coefficient (R=0), it can be found that the increase of the stand-off distance will move the focus point out of the contact point and it will increase the beam spot diameter ao on the glass surface as shown in Fig. 3 (a). As expressed in (1), the peak value of the density Ip at the laser beam center with the Gaussian mode was calculated and shown in Fig. 3 (b) with various stand-off distances Ls and laser powers P. The beam spot diameter ao was also measured with the by the glass and thermal paper and shown in Fig. 4.

TABLE I
Properties of the Ball-Lens [7]

Material	BK7
Density	2510kg/m3
Thermal expansion coefficient	8.6×10-6m/K
Thermal conductivity	1.12W/m- □
Specific heat	710J/kg-K
Melting point	1400 ℃
Tensile strength	30MPa
Rupture strength	690MPa
Young's modulus	8×104MPa
Poisson's ratio	0.208

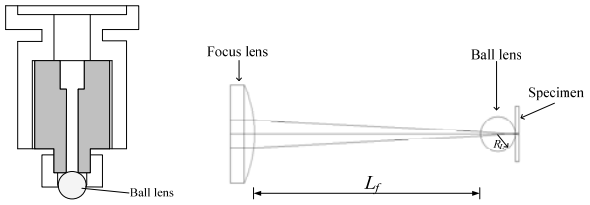

Fig. 2 Lens system for the laser thermal cleavage with a contact ball-lens

$$I_p(x,y) = \frac{(1-R)\times P}{\pi r_0^2} \times \exp^{\left[\frac{-2\times(x^2+y^2)}{r_0^2}\right]} \quad (1)$$

where I_p is the laser intensity (W/m^2). R is the reflectivity. P is the laser power (W). r_o is the radius of the laser beam spot (m).

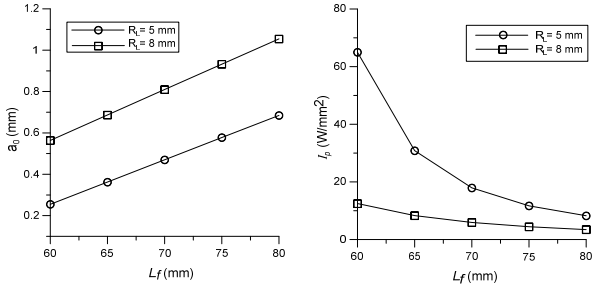

(a) (b)

Fig. 3 Relationships of the beam spot diameter (a), and laser intensity (b) with various stand-off distances and ball diameters

The cutting process could be achieved under various loading of the contact ball-lens on an x-y table. The contact force of the ball-lens in the z-axis was measured by a load cell under the x-y table, and it was calibrated with various settings of in z axis. The process parameters for the present study are listed in Table II.

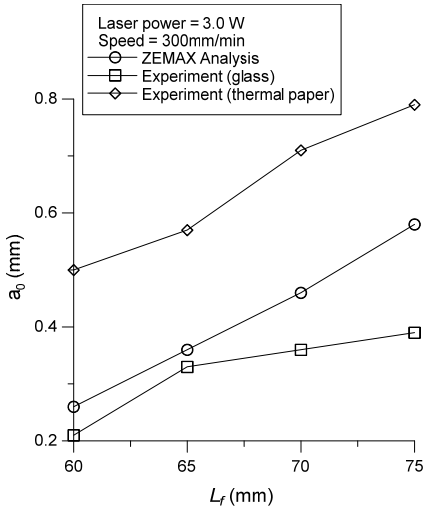

Fig. 4 Relationship between the beam spot diameter and stand-off distance

TABLE II
PROCESS PARAMETERS OF THE LASER CLEAVING

Specimen material	Soda-lime glass
Cutting speed	300 mm/min
Laser power	2W, 2.25W, 2.5W, 2.75W, 3W.
Pre-loads	0N, 5N,10N,15N
Focus lens focal length	70mm
Ball-lens radius	5 mm
L_f	65mm

III. NUMERICAL ANALYSIS

Since the laser cleaving process includes the temperature distribution, stress field and property variation, all of which are significantly inter-related. In order to simplify the analysis, the problem of the laser cleaving on glass sheets herein will be decoupled by two distinct analytical models: the thermal model and the mechanical model in the thermal–elastic numerical analysis. Using the software ANSYS, the element Solid 278 was adopted in the thermal analysis. According to the experimental setup, a half domain of the symmetrical plane with variable mesh grids is shown in Fig. 5, the dimensions of 10 mm x 5 mm x1 mm are selected for the simplicity in computation. A fine meshing around the laser beam was applied to simulate the steep temperature gradients around the heating zone and the number of the meshed elements is 10720. The domain meshes used for the thermal and stress analysis are the same, but the element type was replaced by Solid 185 to calculate the stress and displacement. The temperature dependent properties such as the thermal conductivity, specific heat, Poisson's ratio and Young's modulus of soda-lime glass have been cited from [10] and listed in Table III. Accordingly, the following assumptions are selected in the numerical simulation:

1) The glass properties are homogenous, isotropic and temperature dependent.
2) The laser intensity distribution is Gaussian mode.
3) The thermal boundaries with free convection in the surrounding air are considered.
4) There is no phase change during laser heating.
5) The specimen is annealed before laser cleaving, and its initial condition is free of stress.
6) The stress–strain relationship of the glass substrate is perfectly elastic.
7) Body force has been ignored.

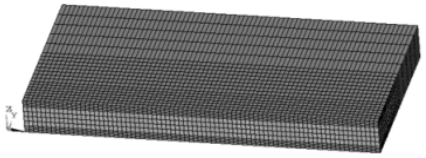

Fig. 5 Grid mesh applied to the stress analysis

TABLE III
PHYSICAL PROPERTIES OF SODA-LIME GLASS [10]

Thermal conductivity , W/mK	1.03
Density, kg/m3	2520
Specific heat, J/kg	800
Thermal expansion coefficient, ×10-6K-1	8.7
Young's modulus, MPa	7160
Poisson ratio	0.23
Softening temperature , oC	730
Average bending fracture strength, MPa	49

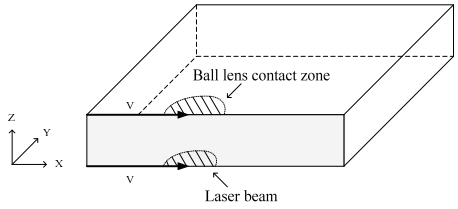

Fig. 6 Physical domain for the stress analysis with laser heating and contact force of the ball-lens

There are numerous factors affect the boundary conditions. The initial temperature of the specimen is assumed to be the ambient temperature of 25°C. The heat convection has been considered from the surface of the glass substrate and the coefficient of the heat convection is quoted as 21W/m2oC on the surfaces including the lower surface of the substrate. On the bottom surface as illustrated in Fig. 5, a circular Nd-YAG laser beam with the Gaussian mode intensity is selected and expressed in (1).

According to the results from ZEMAX for the stand-off distance Lf of 65 mm, the beam spot radius is 0.18 mm for the ball radius of 5 mm as shown in Fig. 3 (a). The substrate was clamped at the lateral sides, except for the leading and trailing edges, which were assumed to be free of stress in the analysis. On the upper surface as illustrated in Fig. 6, the stress loading from the contact ball is expressed in (2) and (3), which is the Hertz equation of the stress distribution between two spheres (or flat plane treated with an infinite large radius) under elastic deformation [11]. Since the cutting path is along the center line of the substrate, a symmetrical domain was selected in the computation and the center line is selected as the x axis and the

displacements were assumed to be constrained at the lateral sides (Ux=Uz=0 at y=5 mm), and the leading and trailing edges are treated as free ends.

$$a = (3F_e A/4k)^{1/3} \quad (2)$$

where a is the radius of the contact region. F_e is the loading force from the contact spheres. $A=(1+\nu_1)/E_1+(1+\nu_2)/E_2$; ν and E are the Possion's ratio and Young's modulus of the corresponding sphere. $k=1/R_1+1/R_2$; R is the radius of the corresponding sphere.

$$P(x,y) = P_0\sqrt{1-\left(\frac{x^2+y^2}{a^2}\right)} \quad (3)$$

where $P_o=3F_e/2\pi a^2$; the maximum contact stress. $P(x, y)$ is the stress distribution in the contact region.

Based on (2), the corresponding radius of the contact region a, and the maximum contact stress Po based on the equation of the Hertz stress are calculated and list in Table IV with various loading for the ball radius of 5 mm.

TABLE IV
THE CONTACT AREA A AND MAXIMUM CONTACT STRESS PO OF THE BALL-LENS WITH VARIOUS LOADINGS ON THE SUBSTRATE

F_e[N]	a [mm]	P_o [MPa]
5	*0.0773*	*399.32*
10	*0.9741*	*503.12*
15	*0.1115*	*575.93*

IV. NUMERICAL RESULTS

With the specified boundary condition, the numerical result for the cutting temperature from the edge of the specimen is shown in Fig. 7. Due to the cooling effects of the surrounding air on the edges, it can be found that the location of the peak temperature of the thermal cycles is close to the laser spot and the peak temperature at the leading edge is about 714°C, which is below the peak temperature of 793°C at the center of the cutting path.

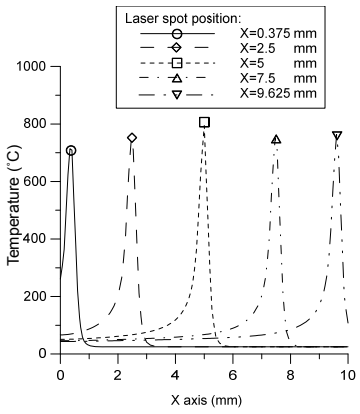

Fig. 7 Temperature profiles of the substrate at various laser positions from the leading edge of the substrate under the laser power of 2.5W

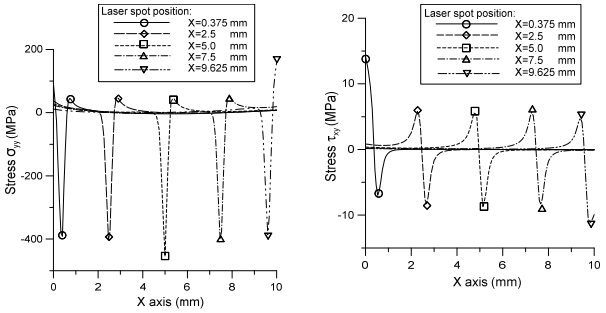

(a) (b)

Fig. 8 States of the normal stress σyy and shear stress τxy along the x axis at various laser positions with the laser power of 2.5W

Based on the fracture modes in the glass cutting with laser, there are two components of the stress states dominating the cleavage process; the opening fracture mode and in-plane shear fracture mode [2]. According to the crack propagation, the normal stress σyy and shear stress τxy in the straight cutting were calculated respectively in the present study. As shown in Fig. 8, the normal stress σyy is in tension and it occurs in front of the laser spot and rapidly changes to the compressive state in the laser center. Similar results for Gaussian beam mode in the glass laser cutting have been found in [6] and the crack formation is mainly based on the opening modes in the cooling stage after the laser passing. According to various laser positions on the bottom surface, the temperature profiles along the cutting path under the laser power of 2.5W, the average of the peak temperatures is around 750oc, and the corresponding stress state of the normal stress and shear stress are shown in Fig. 8 with various laser positions. The magnitude of the compressive stress is about 391 MPa at the laser position of 0.375 mm, and the stress at the leading edge is about 91.7Mpa in tension during the cooling stage. Further results on the shear states are shown in Fig. 8 (b) regarding the change of the stress σxy at various distances to the leading edge of the substrate. As the laser beam passing through these locations, it can be found that the shear stress profiles are similar, except that near the leading edge of the substrate. It can be found that the peak value of the shear stress occurs at the leading edge and is much larger than that near the laser spot.

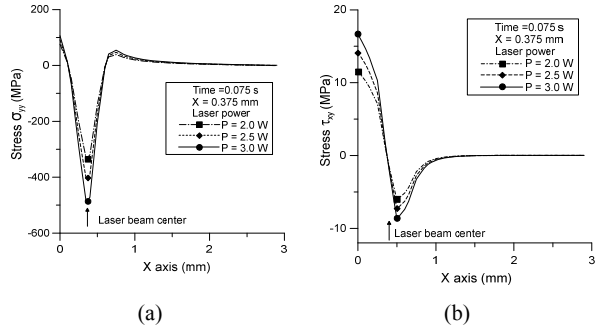

(a) (b)

Fig. 9 Distributions of the normal stress σyy and shear stress τxy along x axis with various laser powers at the beam center of x=0.375 mm

Fig. 9 is the stress profile alone the z axis as the laser beam at the 0.375 mm with various laser powers. It shows that the increase of the laser powers may rise up the magnitude of the compressive stress at the beam center stress. The deviation of the crack propagation in the straight cutting is mainly affected near the edges of the substrate, and similar side cracks occurred at the leading and trailing edges of cutting path [4], [5].

With the various loading forces on the contact zone, the stress analysis has been made and the results are shown in Fig. 10. With the increase of the loading of the ball-lens, the magnitude of the normal and shear stresses are increased. There are tremendous changes of the normal stress distribution in the x axis. However, the effect on the shear stress with the contact loading is not significant.

The normal stress profiles along the z axis at the beam center and leading edge (behind the beam center at x=0.375 mm) with various laser power and contact forces are shown in Figs. 11 and 12 respectively. It can be found that the increase of the tensile stress on the bottom surface (z=0) with the contact force. Furthermore the maximum stress occurs at the leading edge after the laser passing at x=0.375 mm.

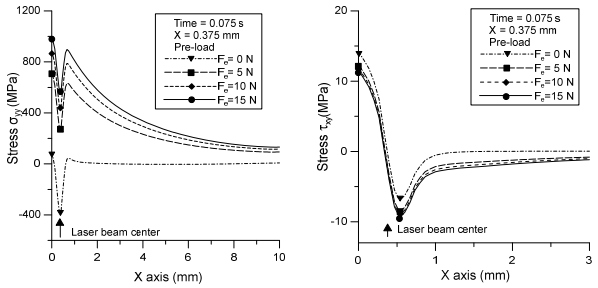

(a) (b)

Fig. 10 Distributions of the normal stress σyy and shear stress τxy along x axis with laser power of 2.5 W and various loadings for the beam center at x=0.375 mm

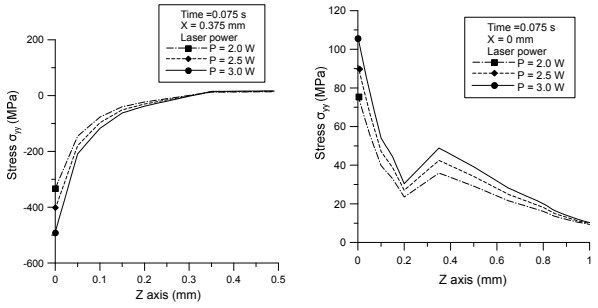

(a) (b)

Fig. 11 Distributions of the normal stress σyy along z axis at the beam center and behind the beam center at x=0.375 mm with variable laser powers.

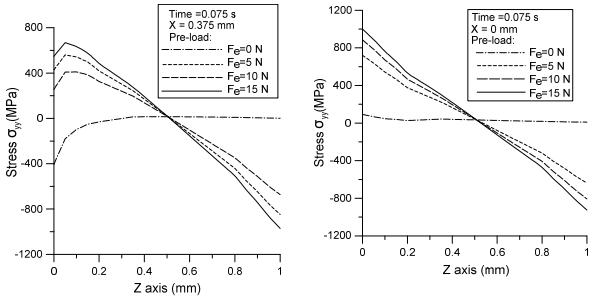

(a) (b)

Fig. 12 Distributions of the normal stress σyy along z axis at the beam center (a) and behind the beam center at x=0.375 mm (b) with variable contact forces

V. Straight-Line Cutting Results

The typical crack patterns in the straight-line cutting are shown in Fig. 13. It can be found that the side crack has always occurred at the leading and trailing edges, but it might randomly appear along the straight-line crack in the middle region (section B). The lengths LA, LB and LC are the regions corresponding to the crack distribution on the leading edge (section A), middle region (section B) and trailing edge (section C).

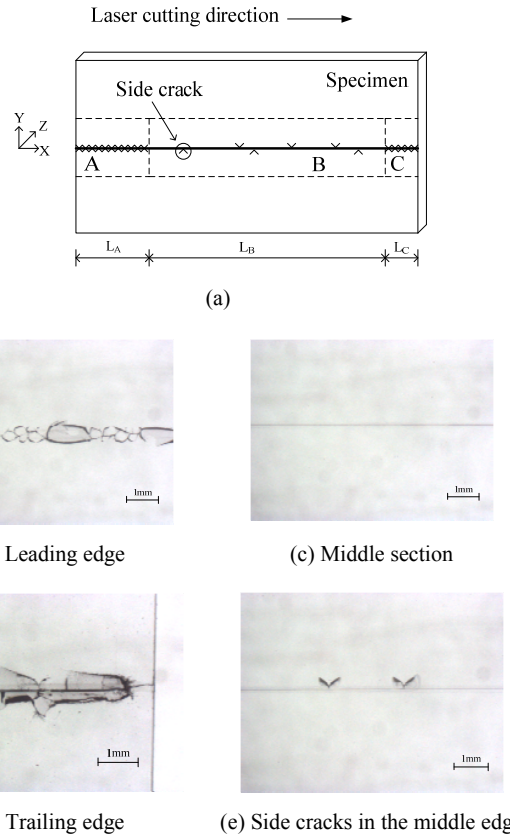

(a)

(b) Leading edge (c) Middle section

(d) Trailing edge (e) Side cracks in the middle edge

Fig. 13 Typical crack patterns in the experiment

Fig. 14 shows the effects of the laser power on the crack

distribution, where the contact force of the ball-lens is set to zero. It can be found that the length LA of the side cracking in the leading edge increases with the laser power as shown in Fig. 14 (a), and the length LB of the straight cut in the middle region increases with the laser power as shown in Fig. 14 (b). Furthermore, there is no clear evidence of the change in the length LC of the cracking region in the trailing edge with the laser power in the present study. It can be found that the length LC is about 5 mm in average under various laser powers in the present study. Fig. 14 (d) shows the amount of the side cracks Ds distributed in the middle region (the length LB) are similar with various laser powers.

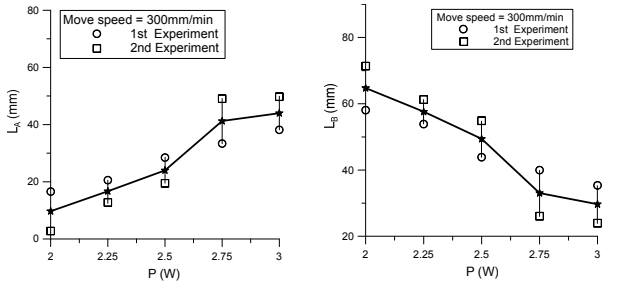

(a) L_a

(b) L_b

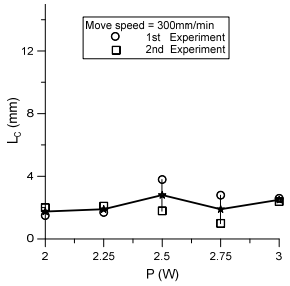

(c) L_c

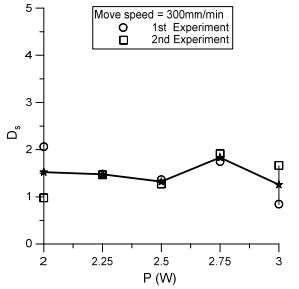

(d) D_s

Fig. 14 Relationships of the length of the cracking regions with various laser powers

As shown in Fig. 15, the length LB of the crack distribution on the middle section at a constant laser power will be increase with various contact forces under 15N. The increase of the ball-lens loading will reduce the length LA, and it will improve the length LB of the straight cut significant as shown in Fig. 15 (b). The length LC of the crack distribution at the trailing edge is not much different under various loadings. However, the amount of the side cracks Ds in the middle region will be affected with a large uncertainty as shown in Fig. 15 (d).

The side view of the crack at the trailing edge is shown in Fig. 16 with the cutting direction on the x axis. The crack width WC defined in Fig. 16 was measured with various loadings of the ball lens.

According to the longitudinal cross-section view of the straight-line crack in the middle region, the depth of the crack hd is denoted in Fig. 16 and measured with various loadings from the contact ball-lens.

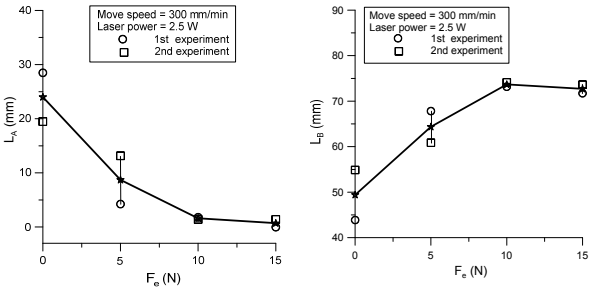

(a) L_a

(b) L_b

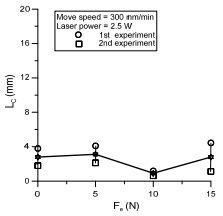

(c) L_c

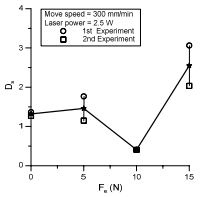

(d) D_s

Fig. 15 Relationship of the length of the cracking regions with various loadings

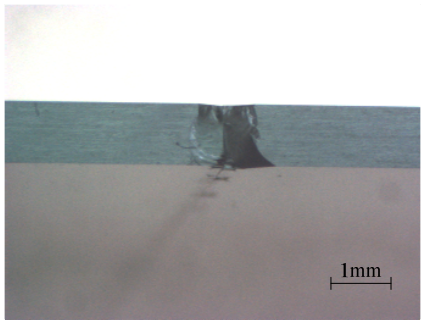

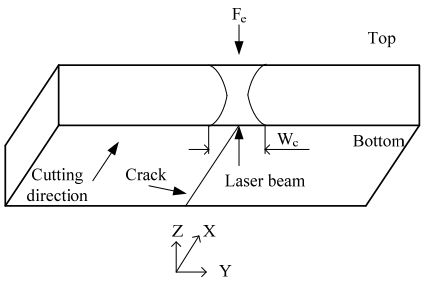

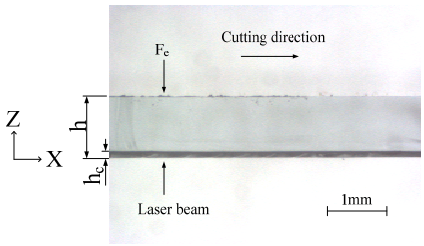

Fig. 16 Definitions of the crack contours

The crack depth of the straight-line cutting in the middle region has been measured and shown in Fig. 17 with various

laser powers. Furthermore, Fig. 18 shows the results of the crack depth hc in the straight cut with various loadings. According to these results, it can be found that the crack depth increases with the laser power below 3.0 W, and similarly with the loading force up to 15 N. The crack depth was measured in the middle region to obtain a uniform distribution. Due to the increase of the tensile stress on the cutting area with the increase of the laser power and ball loading on the bottom surface, the depth growth of the crack is controllable.

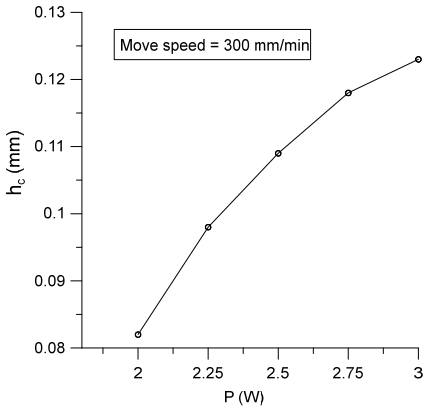

Fig. 17 Relationship of the crack depth with various laser powers

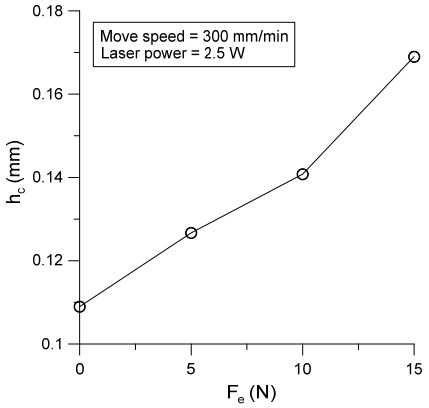

Fig. 18 Relationship of the crack depth with various loadings of the ball-lens

Since the loading force from the ball-lens will significantly rise up the stress state in tension on the bottom surface, it will enhance the crack depth in cutting. In order to characterize the cracking defects in the trailing edge under the laser power and contact loading, the width of the crack-affected zone at the trailing edge was measured and shown in Figs. 19 and 20. It can be found that the loading force from the ball-lens is critical to cause the opening of the crack at the trailing edge as shown in Fig. 21. Apparently the width of the crack affected zone is increased with the loading force. As the loading up to 20 N, an unstable crack occurs frequently at the trailing edge. This type crack is mainly caused by even stress state at the end of the cutting path without the end support on the trailing edge.

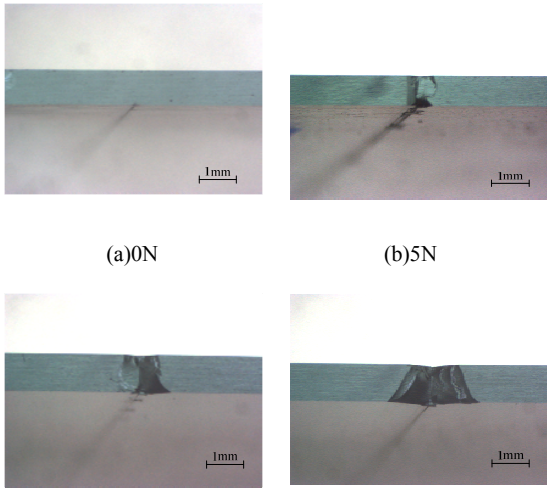

Fig. 19 Photographs of the crack affected zone at the trailing edge

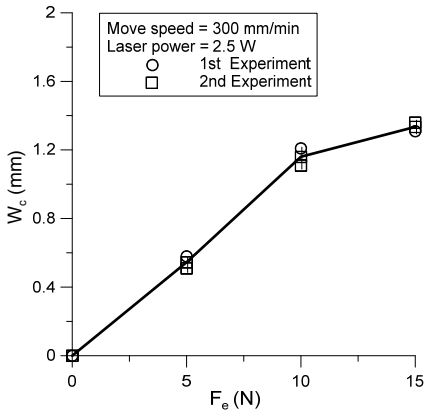

Fig. 20 Relationship of the crack width with various loadings at the trailing edge

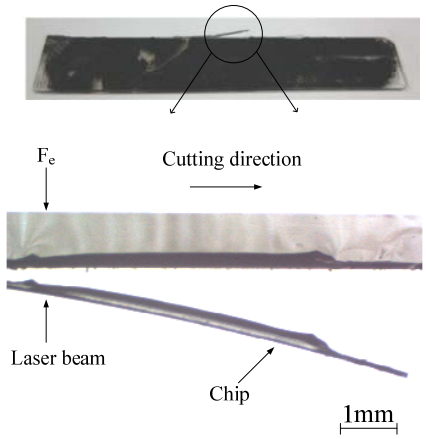

Fig. 21 Typical end cracking with a loading up to 20N

VI. Conclusions

In the straight-line cutting, the crack formation can be found

in the opening mode and dominated by the normal stress, and the side crack would not affected by the shear stress with the laser power and contact force from the ball-lens. The cutting results show that the distributions of the side crack varies with the laser power and contact forces, especially in the leading edge. Therefore, the micro-cracks could be successfully controlled by the ball-lens and affect the cutting quality mainly at the leading edge in the laser cleavage of glass. A comparison between the numerical and experimental results shows that the control of the crack formation mainly depends on the stress states. The tensile stress distribution due to the ball-lens would significantly reduce the amount of the side crack in the leading edge under a certain amount of the contact forces.

REFERENCES

[1] C. H. Tsai,C. J. Chen, "Application of iterative path revision technique for laser cutting with controlled fracture." Optics and Lasers in Engineering, vol. 41, 2004, pp. 189-204.
[2] Y. Miyashita, M. Mogi, H. Hasegawa, S. Sujatanod, Y. Mutoh, "Study on a Controlling Method for Crack Nucleation and Propagation Behavior in Laser Cutting of Glass." Journal of Solid Mechanics and Materials Engineering, vol. 2, 2008, pp. 12.
[3] C. H. Tasi, B. C. Lin, "Laser cutting with controlled fracture and pre-bending applied to LCD glass separation." The International Journal of Advanced Manufacturing Technology, vol. 32,2007,pp. 1155-1162.
[4] S. Nisar, L. Li, M. A. Sheikh, A. J. Pinkerton, "The effect of continuous and pulsed beam modes on cut path deviation in diode laser cutting of glass." International Journal of Advanced Manufacturing Technology, vol. 49, issue 1-4, 2010, pp. 167-175.
[5] S. Nisar, L. Li, M. A. Sheikh, A. J. Pinkerton, S. Safdar, "The effect of laser beam geometry on cut path deviation in diode laser chip-free cutting of glass." Journal of Manufacturing Science and Engineering. Transactions of the ASME, 2010, 132(1):0110021-0110029.
[6] C. H. Tsai, C. S. Liou, "Fracture mechanism of laser cutting with controlled fracture." Journal of Manufacturing Science and Engineering. 125(3) Transactions of the ASME, 2003, pp. 519–528.
[7] S. Yuanyuan, L. Zheng, S. Limin, J. Qiurui, L. Shibo, "Research on the Thermal Effect of Long Pulse Laser Irradiation BK7 Glass." Applied Mechanics and Materials, vol. 347-350, 2013, pp. 1123-1126.
[8] N. Cai, L. J. Yang, Y. Wang, Z. G. Tian," Experimental Research of YAG LaserCutting Soda-lime Glass Sheets with Controlled Fracture." Key Engineering Materials, vol. 431-432, 2010, pp. 507-510.
[9] Crandall SH, Dahl N C, Lardner TJ, (1978) An Introduction to the Mechanics of Solids, McGraw-Hill.
[10] K. Yamamoto, N. Hasaka, H. Morita, E. Ohmura, "Three-dimensional thermal stress analysis on laser scribing of glass." Precision Engineering, vol. 32, 2008, pp. 301-308.
[11] K. L. Johnson, "Contact Mechanics." Press Syndicate of the University of Cambridge. New York, 1985.